Poles tracking of weakly nonlinear structures using a Bayesian smoothing method. (ancien titre Equivalent modal parameters identification using the free decay of a weakly nonlinear structure)

Cyrille Stephan, Hugo Festjens, Franck Renaud, Jean-Luc Dion

Equivalent modal parameters identification using the free decay of a weakly nonlinear structure

Cyrille STEPHAN

Onera - The French Aerospace Lab
F 92322 Châtillon, France

Hugo FESTJENS, Franck RENAUD, Jean-Luc DION

SUPMECA
Saint-Ouen, France

Abstract

This paper describes a method for the identification and the tracking of poles of a weakly nonlinear structure from its free responses. This method is based on a model of multi-channel damped sines whose parameters evolve over time. Their variations are approximated in discrete time by a nonlinear state space model. States are recursively estimated by a new method which couples a two-pass Bayesian estimator with an Expectation-Maximization (EM) algorithm. An iterative procedure between them allows an accurate and robust tracking of poles. As a result, equivalent modal parameters such as frequency and damping are obtained as a function of amplitudes. The method is applied on numerical and experimental cases and show promising results.

Keywords: modal testing, frequency, damping, identification, Unscented Kalman Filter, Expectation-Maximization algorithm

1. Introduction

According to the linear framework in experimental modal analysis, for a given frequency range a structure has a finite set of invariant poles and corresponding shapes. They can be used to model its whole dynamics in this frequency range, taking also into account residual effects due to out-of-frequency-band modes [1].

In reality, invariant poles are unlikely to be observed on experimental results. Most of structural dynamics show a certain degree of nonlinearity, due to materials nature, geometries, joints, friction, impacts, etc. In severe forms of nonlinearities, typical phenomena such as internal resonances, unstable modes may occur and lead the relevancy of modal analysis to questioning. Hence the detection and the identification of nonlinearity is more and more considered as a main step by test engineers [2, 3].

As a general rule, the success of an identification method highly depends on a chosen model and on a specialized algorithm for parameter estimation [4, 5]. Since usual tools of modal analysis aim to get linear modal models, testing the linearity assumption is essential to study their appropriateness on experimental data. Any deviation from expected results that cannot be explained with measurement errors (such as signal noise, reduced observation, ...) is attributed to a lack of good linear behaviour, and then to non-linear dynamics influence. For instance, identifying Frequency Response Functions (FRFs) at different force levels is a simple and efficient way to test the homogeneity (a weak form of linearity) [6]. Another indicator is the coherence function, which gives a scaled degree of linearity over frequency, although it might be misled by some kinds of nonlinearities [2].

However, for many structures, nonlinear forces are often weak compared to linear ones (predominantly mass and stiffness). As a consequence, the linear theory remains relevant for most of industrial structures, since the behaviour of a structure submitted to an external force is close to an equivalent linear one, as long as no bifurcation occurs and nonlinear forces are smooth [7].

Equivalency means here that dynamics analysis can still be reduced to the identification of modes, but these ones are no longer invariant. They depend on the nature of external force and on the structure movement. More specifically, only poles are mainly affected by nonlinearities; except in the case of high energy level, mode shapes barely change and can be regarded as invariant [8].

In the field of signal processing, the problem of identifying variations of poles has often been addressed. Many techniques have been proposed, starting from the Teager energy operator [9, 10]. Feldman proposed the FREEVIB method that uses a Hilbert transform on the free decay and hence obtains the instantaneous characteristics of a mechanical system[11, 12]. When identifying signals coming from free decay, the modulations have to be slower than the carrier as demonstrated by Bedrosian [13], Nuttall [14] and more

recently by Brown[15]. The Empirical Mode Decomposition has been designed by Huang et al. [16, 17, 18] to extract signal components satisfying this requirement before applying the Hilbert transform.

The free decay could also be processed by time-frequency analysis like wavelets [19, 20, 21]. Their high frequency resolution allows an accurate characterization of poles evolution, even though the first periods of free decay are often affected by edge effects. Moreover, when considering a set of several sensors, each signal is processed independently, without using the redundancy of information shared by all sensors. Despite these drawbacks, wavelets were successfully used to extend normal mode appropriation testing to nonlinear systems [7, 22].

This paper is devoted to the analysis of free decay time histories of weakly nonlinear structures. A new method for processing data from multiple sensors will be presented. The response is modelled by multi-channel damped sines whose parameters are recursively estimated over time by a two-pass Bayesian smoothing algorithm based on a Kalman filter. As accurate values are wished from the beginning of signals, an iterative algorithm based on maximization-expectation technique is proposed for obtaining relevant inputs to Kalman filter.

The outline of this paper is as follows. First, a state space in discrete time is introduced for modelling damped waves in section 2. Then instantaneous values of state vector are estimated by a nonlinear version of Kalman filter and an iterative algorithm is proposed in section 3. In section 4, the proposed method is first applied on numerical simulations to assess its efficiency. Finally, an experimental case is studied in section 5.

2. Development of state space model

This part is devoted to the development of a state space model for modelling the temporal evolution and the observation of damped sines. The transition function will be developed in section 2.1 and the observation function in section 2.2.

2.1. Transition function

The free response of a structure, generally produced by a hammer hit or a stepped sine excitation, can be modelled by the sum of S damped sines:

$$x(t) = \sum_{s=1}^{S} A_s^r \exp(\sigma_s t) \cos(\omega_s t + \phi_s) \tag{1}$$

with, for each sine s, A_s^r its corresponding maximum amplitude, ϕ_s its initial phase, ω_s its damped angular frequency and σ_s its damping. For practical reasons, the corresponding analytical signal is more used:

$$x(t) = \sum_{s=1}^{S} A_s \exp\left(\left(\sigma_s + j\omega_s\right) t\right) \tag{2}$$

with each complex amplitude A_s composed of A_s^r and ϕ_s. Equivalent eigenfrequencies and eigendampings are computed by:

$$\omega_{es}^2 = \sigma_s^2 + \omega_s^2 \tag{3}$$
$$\xi_{es} = -\sigma_s/\omega_{es} \tag{4}$$

In discrete time, the response is given by:

$$x(n\Delta t) = \sum_{s=1}^{S} A_s \exp\left(\left(\sigma_s + j\omega_s\right) n\Delta t\right) = \sum_{s=1}^{S} c_{s,n} \tag{5}$$

with Δt the time sampling. One can express $x_n = x(n\Delta t)$ as a function of the previous step:

$$x_n = \sum_{s=1}^{S} A_s \exp\left(\left(\sigma_s + j\omega_s\right)(n-1)\Delta t\right) \exp\left(\left(\sigma_s + j\omega_s\right)\Delta t\right) \tag{6}$$

The transition between two consecutive amplitudes is given by:

$$c_{s,n} = c_{s,n-1} \exp\left(\left(\sigma_s + j\omega_s\right)\Delta t\right) \tag{7}$$

Each complex amplitude is made of real and imaginary parts as $c_{s,n} = a_{s,n} + jb_{s,n}$. Then the previous relation can be written as:

$$\begin{bmatrix} a_{s,n} \\ b_{s,n} \end{bmatrix} = \mathbf{T}_s \begin{bmatrix} a_{s,n-1} \\ b_{s,n-1} \end{bmatrix} \tag{8}$$

with $\mathbf{T}_s$ the transition matrix of damped sine s:

$$\mathbf{T}_s = \exp\left(\sigma_s \Delta t\right) \begin{bmatrix} \cos\left(\omega_s \Delta t\right) & -\sin\left(\omega_s \Delta t\right) \\ \sin\left(\omega_s \Delta t\right) & \cos\left(\omega_s \Delta t\right) \end{bmatrix} \tag{9}$$

It is simply obtained by expanding and combining all terms of equations 7 and 8. This transition matrix $\mathbf{T}_s$ expresses that a wave is damped and rotated between two consecutive time samples [23].

For the general case of M responses, the vector of the complex amplitudes of a damped sine s is:

$$\mathbf{x}_{s,n}^{a} = \left[a_{s,1,n}\ b_{s,1,n}\ a_{s,2,n}\ b_{s,2,n}\ \ldots\ a_{s,M,n}\ b_{s,M,n}\right]^{T} \tag{10}$$

where $\left[a_{s,i,n}\ b_{s,i,n}\right]^{T}$ is the complex amplitude of a damped sine s at time sample n and observation point i. Here the superscript a of $\mathbf{x}_{n,s}^{a}$ denotes the amplitude. Then the function transition for M observations is given by:

$$\mathbf{x}_{s,n}^{a} = \left(\mathbf{I}_{M} \otimes \mathbf{T}_{s}\right) \mathbf{x}_{s,n-1}^{a} \tag{11}$$

since they share the same transition matrix $\mathbf{T}_{s}$. Here the symbol $\otimes$ denotes the Kronecker product and $\mathbf{I}_{M}$ is the identity matrix of size M.

As a free response of a structure generally shows several modes, a vector of S damped sine amplitudes should be considered:

$$\mathbf{x}_{n}^{a} = \begin{bmatrix} \mathbf{x}_{1,n}^{a} \\ \mathbf{x}_{2,n}^{a} \\ \vdots \\ \mathbf{x}_{S,n}^{a} \end{bmatrix} \tag{12}$$

In fact, it only concatenates the $2M$ previous $\mathbf{x}_{s,n}^{a}$ amplitude terms per damped sine.

By combining equations 11 and 12, a relation between two consecutive amplitude vectors is given by:

$$\mathbf{x}_{n}^{a} = \mathbf{\Gamma} \mathbf{x}_{n-1}^{a} \tag{13}$$

with the transition matrix of complex amplitudes:

$$\mathbf{\Gamma} = \begin{bmatrix} \mathbf{I}_{M} \otimes \mathbf{T}_{1} & \mathbf{0}_{2M} & \ldots & \mathbf{0}_{2M} \\ \mathbf{0}_{2M} & \mathbf{I}_{M} \otimes \mathbf{T}_{2} & \ddots & \vdots \\ \vdots & \ddots & \ddots & \mathbf{0}_{2M} \\ \mathbf{0}_{2M} & \ldots & \mathbf{0}_{2M} & \mathbf{I}_{2M} \otimes \mathbf{T}_{S} \end{bmatrix} \tag{14}$$

This transition matrix $\mathbf{\Gamma}$ is made of parameters (angular frequencies $\{\omega_{s}\}$ and dampings $\{\sigma_{s}\}$) which are unknown and have also to be identified. The vector of amplitudes $\mathbf{x}_{n}^{a}$ is concatenated to a vector of parameters which assembles itself all the pulsations and dampings:

$$\mathbf{x}_{n} = \begin{bmatrix} \mathbf{x}_{n}^{p} \\ \mathbf{x}_{n}^{a} \end{bmatrix} \quad \text{with} \quad \mathbf{x}_{n}^{p} = \left[\omega_{1,n}\ \sigma_{1,n}\ \omega_{2,n}\ \sigma_{2,n} \ldots\ \omega_{S,n}\ \sigma_{S,n}\right]^{T} \times \Delta t \tag{15}$$

Parameters are assumed to be almost constant between two samples. As there is no deterministic law for their temporal evolution, here a stochastic framework is chosen to model their variations:

$$\mathbf{x}_n^p = \mathbf{x}_{n-1}^p + \mathbf{w}_{n-1}^p \tag{16}$$

with $\mathbf{w}_n^p$ a random noise which allows parameters to evolve slowly over time.

In conclusion, the dynamical evolution in discrete time is given by

$$\mathbf{x}_n = f\left(\mathbf{x}_{n-1}\right) + \mathbf{w}_{n-1} \tag{17}$$

with the deterministic part given by:

$$f\left(\begin{bmatrix} \mathbf{x}_{n-1}^p \\ \mathbf{x}_{n-1}^a \end{bmatrix}\right) = \begin{bmatrix} \mathbf{I}_{2S} & \mathbf{0}_{2MS} \\ \mathbf{0}_{2S} & \mathbf{\Gamma}_{n-1} \end{bmatrix} \begin{bmatrix} \mathbf{x}_{n-1}^p \\ \mathbf{x}_{n-1}^a \end{bmatrix} \tag{18}$$

where $\mathbf{I}_{2S}$ is the identity matrix of size $2S$. This transition function is nonlinear since, as parameters are allowed to evolve from sample to sample thanks to $\mathbf{w}_n^p$, the matrix $\mathbf{\Gamma}_{n-1}$ depends now on values of parameters given by $\mathbf{x}_{n-1}^p$.

Finally, the random part

$$\mathbf{w}_n = \begin{bmatrix} \mathbf{w}_n^p \\ \mathbf{w}_n^a \end{bmatrix} \tag{19}$$

is modelled by a Gaussian law of zero mean and variance $\mathbf{Q}$. Practical rules for determining relevant value of $\mathbf{Q}$ will be provided in paragraph 3.2.

2.2. Observation function

Let $\mathbf{y}_n$ be the measurement vector of M sensors at sample time n:

$$\mathbf{y}_n = \left[y_{1,n}\ y_{2,n}\ \ldots\ y_{M,n}\right]^T \tag{20}$$

Three types of observation function can be enumerated, depending on the nature of measured quantities : displacement, speed or acceleration. In the simplest case, each sensor gives a displacement at an observation point, with an unavoidable random noise v_i of measurement. Here they are given by the real parts of the complex sines:

$$y_{i,n} = \sum_{s=1}^{S} a_{s,i,n} + v_{i,n} \tag{21}$$

or in a matrix form

$$\mathbf{y}_n = \mathbf{H}\mathbf{x}_n + \mathbf{v}_n \tag{22}$$

The matrix $\mathbf{H}$ is only composed of 0 and 1 necessary to capture all the $a_{s,i,n}$. The observation noise vector $\mathbf{v}_n$ is assumed to be a zero-mean random process of variance $\mathbf{R}$. It could be noticed that, for a displacement sensor, this observation function is linear.

If speed sensors are used, thus the observation function depends on discrete values of $\dot{x}(t)$. For a damped sine in continuous time,

$$\dot{x}(t) = \sum_{s=1}^{S} (\sigma_s + j\omega_s) A_s \exp((\sigma_s + j\omega_s) t) \tag{23}$$

Then in discrete time,

$$\dot{x}_{i,n} = \sum_{s=1}^{S} (\sigma_{s,n} + j\omega_{s,n}) c_{s,i,n} \tag{24}$$

$$\dot{x}_{i,n} = \sum_{s=1}^{S} (\sigma_{s,n} a_{s,i,n} - \omega_{s,n} b_{s,i,n}) + j(\sigma_{s,n} b_{s,i,n} + \omega_{s,n} a_{s,i,n}) \tag{25}$$

Hence the observation function of a speed sensor is given by

$$y_{i,n} = \mathbf{Re}(\dot{x}_{i,n}) + v_{i,n} \tag{26}$$

$$y_{i,n} = \sum_{s=1}^{S} (\sigma_{s,n} a_{s,i,n} - \omega_{s,n} b_{s,i,n}) + v_{i,n} \tag{27}$$

The last case deals with acceleration. Following the same reasoning as for speed sensor, discrete values of $\ddot{x}(t)$ are given by:

$$\ddot{x}_{i,n} = \sum_{s=1}^{S} (\sigma_{s,n} + j\omega_{s,n})^2 c_{s,i,n} \tag{28}$$

and, skipping all the intermediate steps, for an accelerometer the observation function is:

$$y_{i,n} = \left(\sigma_{s,n}^2 - \omega_{s,n}^2\right) a_{s,i,n} - 2\sigma_{s,n}\omega_{s,n} b_{s,i,n} + v_{i,n} \tag{29}$$

It is also possible to combine these three kinds of observation function if heterogeneous sensors are used.

3. Tracking of poles by identification of a state space model

This part is devoted to the use of Kalman filter for the tracking of damped sines based on the state model presented in section 2. The choice of the Unscented Kalman Filter and its corresponding Unscented Rauch-Tung-Striebel Smoother (URTSS) will be presented in section 3.1. Ad-hoc rules of parameterization for the initialization of filtering will be given in section 3.2. Since the first state values and noise covariance matrices have a strong impact on Kalman filtering, a technique for improving their estimation will be proposed in section 3.3. Finally, an iterative algorithm resulting from the previous ideas will be introduced in section 3.4.

3.1. Unscented Kalman Filtering and URTSS

Kalman filtering refers to a family of algorithms which are devoted to the tracking and the estimation of first-order dynamical systems [24]. For known system matrices $\{\mathbf{A}, \mathbf{B}, \mathbf{C}, \mathbf{D}\}$, measured observations $\{\mathbf{y}_n\}$ and inputs $\{\mathbf{u}_n\}$, it estimates a series of state $\{\mathbf{x}_n\}$ which are governed by:

$$\mathbf{x}_n = \mathbf{A}\mathbf{x}_{n-1} + \mathbf{B}\mathbf{u}_{n-1} + \mathbf{w}_{n-1} \tag{30}$$

$$\mathbf{y}_n = \mathbf{C}\mathbf{x}_n + \mathbf{D}\mathbf{u}_n + \mathbf{v}_n \tag{31}$$

where $\mathbf{w}_{n-1}$ is the process noise and $\mathbf{v}_n$ is the measurement noise. It can be proved that the series thus obtained $\{\hat{\mathbf{x}}_n\}$ is the best approximate in the least-squares sense [25].

Although the first version only handles linear system of equations, nonlinear ones were also developed to generalize the range of applications [25]. One of the latest versions, named Unscented Kalman Filtering (UKF), is particularly promising since it can provide satisfying estimates of solutions for an acceptable algorithmic cost. The UKF is basically the combination of the Unscented Transform (UT) with the Kalman filtering [26, 27]. For a system of equations such as:

$$\mathbf{x}_n = f\left(\mathbf{x}_{n-1}, \mathbf{u}_{n-1}, \mathbf{w}_{n-1}\right) \tag{32}$$

$$\mathbf{y}_n = g\left(\mathbf{x}_n, \mathbf{u}_n, \mathbf{v}_n\right) \tag{33}$$

the UT allows estimating the first and second moments of a stochastic variable, even if it is transformed by a nonlinear transition function $f(.)$ or a nonlinear observation function $g(.)$ (see appendix 7.1 for details of computation). Contrary to the linear version, the estimated series $\{\hat{\mathbf{x}}_n\}$ is only optimal at the first order of approximation.

As Kalman filtering was originally used for real-time applications, it only uses past observations. It recursively computes an estimate at time sample n based on the previous estimate $\hat{\mathbf{x}}_{n-1}$ and the new observation $\mathbf{y}_n$. Hence for each time sample, Kalman filtering computes the likeliest distribution, assumed here to be Gaussian, based on current and past observations up to time sample n:

$$p\left(\mathbf{x}_n|\mathbf{y}_{1\to n}\right) \approx N\left(\mathbf{x}_n|\hat{\mathbf{x}}_n, \hat{\mathbf{P}}_n\right) \tag{34}$$

where $\mathbf{y}_{1\to n}$ denotes the reduced set of observations and $N\left(\mathbf{x}_n|\hat{\mathbf{x}}_n, \hat{\mathbf{P}}_n\right)$ is the Gaussian law of mean $\hat{\mathbf{x}}_n$ and variance $\hat{\mathbf{P}}_n$.

Although it can already provide good approximations, better results could be obtained by considering future observations too, since they are available in post-processing analysis. An algorithm named Unscented Rauch-Tung-Striebel Smoother (URTSS) was selected for this task [28]. It involves a separate backward smoothing pass that computes corrections to the first forward filtered data. Therefore the smoothed distribution of states depends, for each time sample, on the whole observations set:

$$p\left(\mathbf{x}_n|\mathbf{y}_{1\to T}\right) \approx N\left(\mathbf{x}_n|\hat{\mathbf{x}}_n^{\natural}, \hat{\mathbf{P}}_n^{\natural}\right) \tag{35}$$

where T is the number of time samples and $\mathbf{y}_{1\to T}$ denotes all measured data. $\hat{\mathbf{x}}_n^{\natural}$ and $\hat{\mathbf{P}}_n^{\natural}$ are the smoothed mean vector and covariance matrix at time sample n. In practice, the URTSS needs the estimated series $\{\hat{\mathbf{x}}_n, \hat{\mathbf{P}}_n\}$ of the first pass and recursively computes $\{\hat{\mathbf{x}}_n^{\natural}, \hat{\mathbf{P}}_n^{\natural}\}$ from $n = T$ to $n = 0$ in a backward manner. For the sake of conciseness, all steps of computation are postponed in appendix 7.2.

In conclusion, the identification of states $\{\mathbf{x}_n\}$ is performed with two successive steps:

1. the UKF computes a first series of estimate $\{\hat{\mathbf{x}}_n\}$ based on past observations $\mathbf{y}_{1\to n}$,
2. the URTSS computes a corrected series of estimate $\{\hat{\mathbf{x}}_n^{\natural}\}$ based on the whole set of observations $\mathbf{y}_{1\to T}$.

Both steps form the two-pass Bayesian smoothing algorithm.

3.2. Initialization of parameters

The recursive computation starts with the initial estimation of $\{\hat{\mathbf{x}}_{\mathbf{0}}, \hat{\mathbf{P}}_0\}$. As previously detailed in paragraph 2.1, the state vector $\mathbf{x}$ combines both parameter values and real-imaginary amplitudes $\mathbf{x} = \left[\left(\mathbf{x}^p\right)^T \quad \left(\mathbf{x}^a\right)^T\right]^T$.

First of all, the number of damped sines should be equal to the number of major peaks in the Power Spectral Densities (PSDs) of signals. It gives the model size directly.

Each damped sine has two terms in the parameter vector:

$$\mathbf{x}^p = \begin{bmatrix} \omega_d \Delta t \\ \sigma \Delta t \end{bmatrix}, \quad \text{with} \quad \begin{cases} \omega_d &= 2\pi f_e \sqrt{1-\xi_e^2} \\ \sigma &= -2\pi f_e \xi_e \end{cases} \tag{36}$$

Here the case of a single damped sine has been chosen for the sake of clarity. A first estimation of f_e is given by picking the major peak in the PSDs. Moreover, an arbitrary value of 1% is used to initialize ξ_e. Although they could seem to be rough estimates for $f_{e,0}$ and ξ_e, they are quite good enough as first values.

Amplitudes stored in vector $\mathbf{x}^a$ are initialized by taking for each measured signal at each selected frequency the corresponding square root amplitudes in the PSDs.

The state covariance matrix P can be initialized by the expected lack of knowledge on states. As for the state vector x, parameters and amplitudes are considered separately:

$$\hat{\mathbf{P}}_0 = \begin{bmatrix} \hat{\mathbf{P}}_0^p & \mathbf{0} \\ \mathbf{0} & \hat{\mathbf{P}}_0^a \end{bmatrix} \tag{37}$$

Uncertainties on the initial frequency δ_f and the initial damping δ_ξ are introduced in the state covariance matrix by:

$$\hat{\mathbf{P}}_0^p = \begin{bmatrix} (2\pi\delta_f \Delta t)^2 & 0 \\ 0 & \left(2\pi \hat{f}_{e,0} \delta_\xi \Delta t\right)^2 \end{bmatrix} \tag{38}$$

where $\hat{f}_{e,0}$ is an initial value of frequency. Typical values of uncertainties are $\delta_f = 1\text{Hz}$ and $\delta_\xi = 1\%$.

The sub-matrix $\hat{\mathbf{P}}_0^a$ contains initial uncertainties on amplitudes. It could be approximated by a fraction of $\mathbf{x_0}^a$.

$$\mathbf{P}_0^a = \text{diag}\left[\left(\frac{\mathbf{x}_0^a}{\delta_x}\right)^2\right] \tag{39}$$

where $\delta_x = 10$ for instance means an initial uncertainty of 10% on amplitudes.

Kalman filtering also relies on two covariance matrices whose values cannot be directly measured : $\mathbf{Q}$ and $\mathbf{R}$. As for the state covariance matrix $\mathbf{P}$, the noise covariance matrix $\mathbf{Q}$ separates parameters and amplitudes components:

$$\mathbf{Q} = \begin{bmatrix} \mathbf{Q}^p & \mathbf{0} \\ \mathbf{0} & \mathbf{Q}^a \end{bmatrix} \tag{40}$$

The matrix $\mathbf{Q}^p$ is a diagonal matrix whose terms are variances of angular frequencies and dampings. A relevant $\mathbf{Q}^p$ is extremely important for the success of Kalman filtering. If the value is too low, the filter is not able to adapt to observations and cannot converge to relevant states. But in the other side, if the value is too high, identified parameters may evolve too fast and are not representative of an expected evolution. Then finding good values for $\mathbf{Q}^p$ is often one of the main points of Kalman filtering [25].

It will always be assumed that a diagonal matrix form is suitable for $\mathbf{Q}^p$ without lack of generality. For instance, for $S = 1$, i.e. one damped sine

$$\mathbf{Q}^p = \begin{bmatrix} q_\omega & 0 \\ 0 & q_\sigma \end{bmatrix} \tag{41}$$

The first state, namely the angular frequency ω_n times the time step Δt, is able to evolve by a random walk:

$$\omega_n \Delta t = \omega_{n-1} \Delta t + \epsilon_n \tag{42}$$

where $\epsilon_n = N(0, q_\omega)$ allows for a slight evolution of ω_n over a time step. During the whole response, the final value ω_N is given by N successive steps:

$$\omega_N = \hat{\omega}_0 + \frac{1}{\Delta t} \sum_{n=1}^{N} \epsilon_n \tag{43}$$

As a relevant value for q_ω could be obtained by assuming a regular evolution over N steps with the same standard deviation $\sqrt{q_\omega}$, then:

$$\omega_N = \hat{\omega}_0 + \frac{1}{\Delta t} \sum_{n=1}^{N} \sqrt{q_\omega} \tag{44}$$

$$\omega_N = \hat{\omega}_0 (1 + V_f) \tag{45}$$

where V_f is the frequency variation of a structure response during a free decay. Hence

$$q_\omega = \left(\frac{V_f \hat{\omega}_{e,0} \Delta t}{N} \right)^2 \tag{46}$$

For most structures which have nonlinear joints, frequency variations such as $V_f = 5\%$ are common.

By analogy, a similar expression is given for σ:

$$q_\sigma = \left(\frac{V_\xi \hat{\xi}_0 \hat{\omega}_{e,0} \Delta t}{N} \right)^2 \tag{47}$$

Contrary to frequency, a damping ratio ξ is known to experience significant variations in function of amplitude. As typical eigendamping ranges in value from 1 to 5%, $V_\xi = 5$ enables the Kalman filtering to start at 1% and finishes at 5%.

In the case of a free response, $\mathbf{Q}^a$ should be a null matrix as there is no external excitation. But giving a non-zero value to $\mathbf{Q}^a$, even very small, ensures flexibility and stability in Kalman filtering. Hence a diagonal matrix $\mathbf{Q}^a = \mathbf{I}\epsilon$ is chosen for this purpose, with ϵ is a small value which depends on the accuracy of the used computer.

The matrix of observation noise variances $\mathbf{R}$ can be estimated by knowing the characteristics of used sensors. If they are not available, rough estimates can be given by a percentage of signals variances. For instance, if $\mathbf{R} = (0.01)^2 * \mathrm{var}(\mathbf{y})$ for a single sensor, then it is assumed that the Signal on Noise Ratio is 1%.

3.3. Expectation-Maximization algorithm for noise covariances estimation

Although formulae introduced in paragraph 3.2 often give satisfying values for $\{\mathbf{Q}, \mathbf{R}, \mathbf{x}_0, \mathbf{P}_0\}$, it is advisable to improve their estimation as well as possible. Indeed they are directly used as inputs for the two-pass Bayesian smoothing algorithm, and therefore states estimates strongly depend on them. In this work their values are optimized thanks to the Expectation-Maximization (EM) algorithm [29]. This technique was initially designed for the linear Kalman filter, and then adapted to the Extended Kalman filter [30]; here it is proposed to extend it to the Unscented Kalman Filter.

Let $\mathbf{\Theta} = \{\mathbf{x}_0, \mathbf{P}_0, \mathbf{Q}, \mathbf{R}\}$ be the set of parameters that are unknown and $\{\mathbf{X}_N, \mathbf{Y}_N\} = (\mathbf{x}_1, \ldots, \mathbf{x}_N, \mathbf{y}_1, \ldots, \mathbf{y}_N)$ contain the true states and observations set of the system. The set of parameters $\mathbf{\Theta}$ will be estimated under the maximum likelihood framework by maximising the log-likelihood function:

$$\max_{\mathbf{\Theta}} \quad \log L\left(\mathbf{\Theta} | \mathbf{X}_N, \mathbf{Y}_N\right) = \log p\left(\mathbf{X}_N, \mathbf{Y}_N | \mathbf{\Theta}\right) \tag{48}$$

where $p\left(\mathbf{X}_N, \mathbf{Y}_N|\mathbf{\Theta}\right)$ is the joint probability density function:

$$\begin{aligned} p\left(\mathbf{X}_N, \mathbf{Y}_N|\mathbf{\Theta}\right) &= \frac{1}{2\pi|\mathbf{P}_0|^{1/2}} \exp\left(-\frac{\left(\mathbf{x}_0-\mu_0\right)^T \mathbf{P}_0^{-1}\left(\mathbf{x}_0-\mu_0\right)}{2}\right) \\ &\times \prod_{n=1}^{N} \frac{1}{(2\pi)^{S(M+1)}|\mathbf{Q}|^{1/2}} \exp\left(-\frac{\mathbf{e}_n^T\mathbf{Q}^{-1}\mathbf{e}_n}{2}\right) \\ &\times \prod_{n=0}^{N} \frac{1}{(2\pi)^{M/2}|\mathbf{R}|^{1/2}} \exp\left(-\frac{\mathbf{v}_n^T\mathbf{R}^{-1}\mathbf{v}_n}{2}\right) \end{aligned} \tag{49}$$

where $|.|$ is the determinant of a matrix. As the true set $\{\mathbf{X}_N, \mathbf{Y}_N\}$ is not available, Shumway and Stoffer proposed an iterative approach based on an EM technique which works on the conditional expectation of $\log L\left(\mathbf{\Theta}|\mathbf{X}_N, \mathbf{Y}_N\right)$ (see [29]). Although this method was initially designed for the linear Kalman filter, its nonlinear version is derived here thanks to the Unscented Transform.

Given the current value of $\mathbf{\Theta}^{(j)} = \{\mathbf{x}_0^{(j)}, \mathbf{P}_0^{(j)}, \mathbf{Q}^{(j)}, \mathbf{R}^{(j)}\}$ and the observation set $\mathbf{Y}_N$, a data set $\hat{\mathbf{X}}_N^{(j)} = \left(\hat{\mathbf{x}}_{0|N}^{(j)}, \ldots, \hat{\mathbf{x}}_{N|N}^{(j)}\right)$ is generated by the two-pass Bayesian smoothing algorithm. At the jth iteration, the expectation of $\log L\left(\mathbf{\Theta}|\mathbf{X}_N, \mathbf{Y}_N\right)$ conditioned to $\mathbf{Y}_N$ and $\mathbf{\Theta}^{(j)}$ is given as:

$$\begin{aligned} E\left[\log L\left(\mathbf{\Theta}|\mathbf{X}_N, \mathbf{Y}_N\right)\right] &= -\log|\mathbf{P}_0| - N\log|\mathbf{Q}| \\ &-\mathrm{tr}\left[\mathbf{P}_0^{-1}\left(\mathbf{P}_{0|N}^{(j-1)} - \left(\mathbf{x}_{0|N}^{(j)} - \mathbf{x}_0\right)\left(\mathbf{x}_{0|N}^{(j)} - \mathbf{x}_0\right)^T\right)\right] \\ &-\mathrm{tr}\left[\mathbf{Q}^{-1}\left(\mathbf{B}_1^{(j)} - \mathbf{B}_2^{(j)} - \left(\mathbf{B}_2^{(j)}\right)^T + \mathbf{B}_3^{(j)}\right)\right] \\ &-\mathrm{tr}\left[\mathbf{R}^{-1}\left(\mathbf{B}_4^{(j)} - \mathbf{B}_5^{(j)} - \left(\mathbf{B}_5^{(j)}\right)^T + \mathbf{B}_6^{(j)}\right)\right] \end{aligned} \tag{50}$$

where matrices $\{\mathbf{B}_i\}, i = 1..6$ are given in appendix 7.4.

Secondly, the likelihood $E\left[\log L\left(\mathbf{\Theta}|\mathbf{X}_N, \mathbf{Y}_N\right)\right]$ is maximized by taking the partial derivatives with respect to $\mathbf{Q}$ and $\mathbf{R}$ and setting them to zero:

$$\mathbf{Q}^{(j+1)} = \frac{1}{N}\left(\mathbf{B}_1^{(j)} - \mathbf{B}_2^{(j)} - \left(\mathbf{B}_2^{(j)}\right)^T + \mathbf{B}_3^{(j)}\right) \tag{51}$$

In part 3.2, a splitting in two diagonal parts has been assumed for the noise covariance matrix $\mathbf{Q}$:

$$\mathbf{Q} = \begin{bmatrix} \mathbf{Q}^p & \mathbf{0} \\ \mathbf{0} & \mathbf{Q}^a \end{bmatrix} \tag{52}$$

In practice, it is better to update the diagonal terms of the sub-matrix $\mathbf{Q}^p$ only and to keep the sub-matrix $\mathbf{Q}^a$ to a constant value. If we denote with a superscript p the corresponding left-upper sub-matrices of $\mathbf{B}_1$,$\mathbf{B}_2$ and $\mathbf{B}_3$, the update of $\mathbf{Q}$ can be restricted to:

$$\mathbf{Q}^{p,(j+1)} = \frac{1}{N}\text{diag}\left[\left(\mathbf{B}_1^{p,(j)} - \mathbf{B}_2^{p,(j)} - \left(\mathbf{B}_2^{p,(j)}\right)^T + \mathbf{B}_3^{p,(j)}\right)\right] \tag{53}$$

and the matrix $\mathbf{Q}^a$ is unchanged. The update of the noise measurement matrix $\mathbf{R}$ is performed with:

$$\mathbf{R}^{(j+1)} = \frac{1}{N}\left(\mathbf{B}_4^{(j)} - \mathbf{B}_5^{(j)} - \left(\mathbf{B}_5^{(j)}\right)^T + \mathbf{B}_6^{(j)}\right) \tag{54}$$

Contrary to the noise covariance matrix $\mathbf{Q}$, extra-diagonal terms may appear in $\mathbf{R}$, allowing then the potential cross-terms of noise between different sensors.

Since it is not possible to isolate the initial mean $\mathbf{x}_0$ and covariance matrice $\mathbf{P}_0$ in equation 50, the updates are simply made by taking their last estimated values provided by the URTSS at the previous iteration:

$$\mathbf{x}_0^{(j+1)} = \hat{\mathbf{x}}_{0|N}^{(j)} \quad \text{and} \quad \mathbf{P}_0^{(j+1)} = \hat{\mathbf{P}}_{0|N}^{(j)} \tag{55}$$

3.4. Final algorithm

The resulting method is an iterative process which alternates between the two-pass Bayesian algorithm and the maximum likelihood estimator with the EM technique as follows.

1. Initialize the set of parameters $\mathbf{\Theta}^{(0)} = \{\mathbf{x}_0, \mathbf{P}_0, \mathbf{Q}, \mathbf{R}\}$ by using formulae of paragraph 3.2.
2. Using the set $\mathbf{\Theta}^{(j)}$, compute a set of states $\hat{\mathbf{X}}_N$ by applying the UKF.
3. Improve the results by applying the URTSS.
4. Expectation step : the smoothed state values are used to compute the matrices of maximum likelihood thanks to the UT $\{\mathbf{B}_1^{(j)}, \ldots, \mathbf{B}_6^{(j)}\}$.
5. Maximization step : the estimates of the parameters $\{\mathbf{x}_0, \mathbf{P}_0, \mathbf{Q}, \mathbf{R}\}$ are updated to get $\mathbf{\Theta}^{(j+1)}$.
6. Repeat Steps 2-4 until convergence.

The iterations are ended if a maximum number of iterations is reached or if the following criterion is satisfied

$$\frac{\|\mathbf{p}^{(j)} - \mathbf{p}^{(j-1)}\|}{\|\mathbf{p}^{(j-1)}\|} < \epsilon \tag{56}$$

where $\mathbf{p}$ denotes a poles series ($\{-\xi\omega + i\omega\sqrt{1-\xi^2}\}$) and ϵ is a small positive number.

4. Simulation results

4.1. Numerical model

The numerical case is an one-degree-of-freedom system

$$m\ddot{x} + c\dot{x} + kx + r(t) = f_e(t) \tag{57}$$

where $m = 1$, $c = 2m\xi_0\omega_0$, $k = m\omega_\infty$ and $r(t)$ is the restoring force due to an Iwan model (see figure 1). The Iwan model is a parallel association of N_J Jenkins elements, each of them being a series association of a linear spring of stiffness σ/N_J and a Coulomb slider of breaking force F_j. The restoring force of each Jenkins element is simulated by a modified Dahl formulation (see [31])

$$\dot{r_j} = \frac{\sigma}{N_J}\left|1 - \frac{r_j}{F_j}sgn(\dot{x})\right|^\alpha sgn\left(1 - \frac{r_j}{F_j}sgn(\dot{x})\right)\dot{x} \tag{58}$$

where α is a small exponent.

The system is assumed to be observed with four accelerometers

$$\ddot{y} = \Phi\ddot{x} + v, \quad \Phi = \begin{bmatrix} 3 & 2 & 8 & 6 \end{bmatrix} \tag{59}$$

where v is the noise observation vector such as 1% of random noise is added to signals.

The values of $\{r_m, \sigma, \xi_0, \omega_0, \omega_\infty\}$ are chosen in order to have an evolution of equivalent modal parameters as a function of accelerometer 1 amplitude such as presented on figure 2.

4.2. Application of the methodology

The system is excited by a Morlet wavelet whose central frequency is 15 Hz. The accelerations generated by this excitation force are simulated on 10 seconds and depicted on figure 3. A white noise is added to signals in order to obtain realistic measured signals. The ratio of standard deviation between the added noise and the free-noise signals is about 1%.

A clarification should be made on the transient part due to the wavelet (see figure 4). In fact, a wavelet has a short but not negligible time of fading down. Although signals used for identification may begin at the maximum

of amplitude, the free response starts approximately one period later, when the excitation force is close to nil. Then there is one period of signals which could be used for post-processing, but irrelevant for final results presentation since the system is not exactly free during this period.

Results of the proposed algorithm are depicted on figure 5. Equivalent modal parameters are identified as a function of time for the whole system, and amplitudes are computed for each sensor. It can be firstly noticed that strong variations occur in a short temporal frame (one second in this example) compared to the whole range of time. It emphasizes the need to identify the first periods as well as possible.

The speed of convergence is studied by depicting the first and last results on figure 6. Two curves show the results of the first iteration : the first pass (UKF) and the second pass (URTSS). The third curve gives the results of the 7th iteration (last two-pass Bayesian smoothing). Intermediate results are not shown since most significant variations are observed during the first pass of Kalman filtering and the second pass of Bayesian smoothing.

By representing the equivalent modal parameters as a function of an accelerometer amplitude (numbered 1 here), a comparison with the reference curves is plotted on figure 7. These reference curves were obtained by using the harmonic balance method on the system [32]. Very accurate matching is obtained for both frequency and damping variations. Maximum error deviations are about 0.01 Hz on frequency and 0.1% on damping.

4.3. Discussion

Three main reasons could be enumerated to explain the small deviations. Firstly, the reference curves are not the theoretical evolutions for this excitation since no closed form solutions are known. Instead we use evolutions obtained for a harmonic evolution, and equivalent modal parameters calculated for a sine excitation are not exactly equal to the ones of a free response.

Secondly, although the Runge-Kutta solver is very accurate, a trade-off between instantaneous frequency and damping is made at each time step and resulting numerical errors are unavoidable during simulation.

Finally, the identification algorithm has also its own limitations and accuracy. Nevertheless, such deviations are very low and could be considered as acceptable.

An additional check of performance is given by synthesizing the accelerations based on identified states (from the final iteration) and comparing them to noise-free and noisy accelerations signals. For example, on figure 8 these

three cases are plotted for the accelerometer 1. At the beginning (left part), all amplitudes match well, since the amplitude on noise ratio is high and the first states have been correctly estimated by the algorithm. Furthermore, even if noise amplitude is more significant at low amplitude (right part of the figure), the method still provides accurate states since the synthesized acceleration matches the noise-free acceleration well.

5. Experimental application

5.1. H Bench

The experimental rig consists of two beams linked by a lap-joint and two seismic masses (see figure 9). All of them are made of steel. The seismic masses and the beam are glued together and tightened with one M10 bolt on each side. The glue associated with a strong clamping of the M10 bolts ensures a very weak damping. The joint itself is assembled with two M6 bolts in the center of the overlap and four M4 bolts close to the edges.

This bench is designed to load the joint either on a torsional or on a bending motion thanks to the two first modes. A FE model gives these two modes in free boundary conditions at 50 and 90 Hz (see figure 10). The third mode, namely the second bending mode, has a natural frequency above 200 Hz.

According to the FE model, the torsion and bending modes have two common nodes where their nodal lines intersect. The free boundary conditions are obtained by hanging the structure with nylon cables at these points.

The torsion and bending modes have very low amplitude at joints between the lap-joint and the masses (around the M10 bolts). So it is expected that the M10 bolts have very low influence on the vibratory dissipation of these modes. On the other hand, the M6 and M4 bolts located on the lap-joint should have a significant impact on the poles.

For each mode, the hit position is at the intersection of the maximum amplitude of the studied mode and of the nodal line of the other mode (named H1 and H2 points on figure 10). The hammer mass and its flexibility tip are chosen to have a cutting frequency just over the second mode (> 100 Hz). Then hitting the structure at these two points enabled us to highlight as well as possible the bending and torsion modes separately.

Accelerations are measured at six points along the beam (Acc1 to Acc6) and at one point on the seismic mass (Acc7). Residual participations of low

dynamic rigid motions and higher-order modes are removed from signals by applying a FIR band-pass filter.

5.2. Results

A hammer hit is applied on the H2 point of the structure to excite the bending mode and measured signals are processed by the proposed methodology. Then equivalent modal parameters values are obtained per time sample, together with amplitude level per damped sine and per signal (see figure 11). As for the numerical case in section 4, most variations occur during a short period of time at the beginning of the decay. In fact, the most useful information is located in the first 0.5 s. Then the fast convergence of the UKF and the corrections due to the URTSS allow identifying the parameters accurately, even in a short time frame.

As a better presentation, the previous equivalent modal parameters are plotted as a function of Acc1 displacement amplitude on figure 12. The frequency lowers as a function of amplitude level, while damping ratio grows. Such variations are typical of the influence of dry friction on modal parameters.

Four hits of hammer were applied on the H1 point and all sets of measured signals were processed according to the same methodology (see figure 13). Curves match very well, which shows the good repeatability of the tests, even if the force level is not constant. It can be noticed that the level of hammer hit impulse has a slight effect on the equivalent modal parameters. For example, the hit 4, which is the strongest one since it gives the maximum amplitude of displacement, has always lower frequency and higher damping values compared to the three other cases. Anyway these deviations are very low and can be considered as acceptable.

The influence of the M4 bolts torque is studied by estimating the equivalent parameters of the torsion mode for three tightening cases of the four M10 bolts: 0.5, 1 and 2 Nm. For each case, several hits were performed for evaluating the repeatability of tests (see figure 14). For each tightening case, all curves of equivalent parameters match very well, since the deviations are about 0.3 Hz for frequency and 0.5% for damping, considering that they evolve strongly in the range 39-45 Hz for the frequency and 0.5-5.7 % for the damping ratio. As a result, the influence of tightening is easily identified.

At 0.5Nm, the friction due to lap-joint movement has a maximum impact at 0.25 mm of Acc7 displacement. At 1 and 2 Nm, the frequency lowers and the damping ratio grows continuously as a function of amplitude. As a

rule, the stronger the torque is, the less influential it is on equivalent modal parameters. In the extreme case of tightening, these ones should be constant and the structure dynamics should be linear, as if the whole structure was only one block of steel.

6. Conclusion

The aim of this study was to present a new method for the identification of equivalent modal parameters from free responses of structures. A state space model was expressed in order to model the discrete time evolution of damped sines. Frequency and damping were integrated in the state vector, so that their instantaneous values can be identified. Different observation functions were proposed depending on the type of used sensors. The tracking of state vector was performed by an Unscented Kalman Filter followed its corresponding Unscented Rauch-Tung-Striebel Smoother. As accurate identified states are required from the beginning of signals decay, an iterative algorithm was proposed for estimating first values of state vector and noise covariances matrices.

The proposed method was applied and assessed on numerical and experimental cases. Results showed that equivalent modal parameters as a function of amplitude level can be obtained accurately. More specifically, satisfying states are estimated since the beginning of signals, thus providing equivalent modal parameters even at high level amplitude.

7. Appendixes

7.1. The Unscented Transform

The Unscented Transform (UT) is a deterministic sampling technique which computes a minimal set of sigma points $\{\mathbf{x}^{(i)}\}$ around a density probability function of mean $\mathbf{x}$ and covariance $\mathbf{P}$:

$$\{\mathbf{x}^{(i)}\} = \begin{bmatrix} \mathbf{x} & \mathbf{x} + \gamma \left(\mathbf{P}\right)^{1/2} & \mathbf{x} - \gamma \left(\mathbf{P}\right)^{1/2} \end{bmatrix} \quad i = 0 \dots 2L \tag{60}$$

where $(\mathbf{P})^{1/2}$ denotes the Cholesky decomposition of $\mathbf{P}$. Rules for obtaining a relevant value of γ are given in [27]. It can be easily proved that the mean and covariance of this computed set of samples match the initial mean $\mathbf{x}$ and covariance $\mathbf{P}$. The UT is extensively used in the Unscented Kalman Filter and its related Unscented Rauch-Tung-Striebel smoother.

7.2. Unscented Kalman filter

The Kalman filter estimates the dynamic evolution of a probability density function (mean $\hat{\mathbf{x}}_n$ and covariance $\hat{\mathbf{P}}_n$) at step n based on previous step $n-1$. Knowing a first couple $\{\hat{\mathbf{x}}_0, \hat{\mathbf{P}}_0\}$, it is applied from $n=1$ up to $n=T$ in two major phases : prediction and update.

Prediction phase

1. Creation of a sigma points set $\{\mathbf{x}_{n-1}^{(i)}\}$ from $\hat{\mathbf{x}}_{n-1}$ and $\hat{\mathbf{P}}_{n-1}$ by formula 60
2. Each point is propagated through the transition function :

$$\mathbf{x_{n|n-1}^{(i)}} = f\left(\mathbf{x_{n-1}^{(i)}}\right), \quad i = 0 \dots 2L \tag{61}$$

3. The predicted state estimate is computed as :

$$\hat{\mathbf{x}}_{\mathbf{n}}^{-} = \sum_{i=0}^{2L} W_i^{(m)} \mathbf{x_{n|n-1}^{(i)}} \tag{62}$$

4. The predicted covariance estimate is given by :

$$\hat{\mathbf{P}}_{\mathbf{n}}^{-} = \sum_{i=0}^{2L} W_i^{(c)} \left(\mathbf{x_{n|n-1}^{(i)}} - \hat{\mathbf{x}}_{\mathbf{n}}^{-}\right)\left(\mathbf{x_{n|n-1}^{(i)}} - \hat{\mathbf{x}}_{\mathbf{n}}^{-}\right)^T + \mathbf{Q} \tag{63}$$

Update phase

5. Creation of a new set of sigma points $\{\mathbf{x}_{n-1}^{(i)}\}$ from $\hat{\mathbf{x}}_{n-1}^{-}$ and $\hat{\mathbf{P}}_{n-1}^{-}$ by formula 60
6. Application of the observation function on each point :

$$\mathbf{y_{n|n-1}^{(i)}} = g\left(\mathbf{x_{n|n-1}^{(i)}}\right), \quad i = 0 \dots 2L \tag{64}$$

7. The predicted observation is computed as :

$$\hat{\mathbf{y}}_{\mathbf{n}}^{-} = \sum_{i=0}^{2L} W_i^{(m)} \mathbf{y_{n|n-1}^{(i)}} \tag{65}$$

8. The innovation covariance is calculated by :

$$\hat{\mathbf{P}}_{\mathbf{yy,n}} = \sum_{i=0}^{2L} W_i^{(c)} \left[\mathbf{y}_{\mathbf{n|n-1}}^{\mathbf{(i)}} - \hat{\mathbf{y}}_{\mathbf{n}}^{-}\right] \left[\mathbf{y}_{\mathbf{n|n-1}}^{\mathbf{(i)}} - \hat{\mathbf{y}}_{\mathbf{n}}^{-}\right]^T + \mathbf{R} \tag{66}$$

9. The cross covariance matrix is given by :

$$\hat{\mathbf{P}}_{\mathbf{xy,n}} = \sum_{i=0}^{2L} W_i^{(c)} \left[\mathbf{x}_{\mathbf{n|n-1}}^{\mathbf{(i)}} - \hat{\mathbf{x}}_{\mathbf{n}}^{-}\right] \left[\mathbf{y}_{\mathbf{n|n-1}}^{\mathbf{(i)}} - \hat{\mathbf{y}}_{\mathbf{n}}^{-}\right]^T \tag{67}$$

10. The Kalman gain is computed as :

$$\mathbf{K_n} = \hat{\mathbf{P}}_{\mathbf{xy,n}} \hat{\mathbf{P}}_{\mathbf{yy,n}}^{\mathbf{-1}} \tag{68}$$

11. The updated state estimate is calculated by :

$$\hat{\mathbf{x}}_{\mathbf{n}} = \hat{\mathbf{x}}_{\mathbf{n}}^{-} + \mathbf{K_n} \left(\mathbf{y_n} - \hat{\mathbf{y}}_{\mathbf{n}}^{-}\right) \tag{69}$$

12. The updated covariance matrix is computed as :

$$\hat{\mathbf{P}}_{\mathbf{n}} = \hat{\mathbf{P}}_{\mathbf{n}}^{-} - \mathbf{K_n} \hat{\mathbf{P}}_{\mathbf{yy,n}} \mathbf{K_n^T} \tag{70}$$

Rules for computing $W_i^{(c)}$ and $W_i^{(m)}$ are given in [27].

7.3. Rauch-Tung-Striebel smoother

Contrary to Kalman filter, the Rauch-Tung-Striebel smoother processes data in a recursive manner. The followings steps are performed on $\{\hat{\mathbf{x}}_n, \hat{\mathbf{P}}_n\}$, starting at $n = T - 1$ and ending at $n = 0$.

1. Creation of a set of sigma points $\{\mathbf{x}_n^{(i)}\}$ from $\hat{\mathbf{x}}_n$ and $\hat{\mathbf{P}}_n$ by formula 60
2. Propagate the sigma points through the transition function :

$$\hat{\mathbf{x}}_{\mathbf{n+1|n}}^{\mathbf{(i)}} = f\left(\hat{\mathbf{x}}_{\mathbf{n}}^{\mathbf{(i)}}\right), \quad i = 0 \ldots 2L \tag{71}$$

3. The predicted mean is computed as :

$$\hat{\mathbf{x}}_{\mathbf{n+1|n}}^{\natural} = \sum_{i=0}^{2L} W_i^{(m)} \hat{\mathbf{x}}_{\mathbf{n+1|n}}^{\mathbf{(i)}} \tag{72}$$

4. The predicted covariance matrix is calculated by :

$$\hat{\mathbf{P}}_{\mathbf{n+1|n}}^{\natural} = \sum_{i=0}^{2L} W_i^{(c)} \left(\hat{\mathbf{x}}_{\mathbf{n+1|n}}^{\mathbf{(i)}} - \hat{\mathbf{x}}_{\mathbf{n+1|n}}^{\natural}\right) \left(\hat{\mathbf{x}}_{\mathbf{n+1|n}}^{\mathbf{(i)}} - \hat{\mathbf{x}}_{\mathbf{n+1|n}}^{\natural}\right)^T \tag{73}$$

5. The cross covariance matrix is computed as :

$$\hat{\mathbf{S}}^{\natural}_{\mathbf{n+1|n}} = \sum_{i=0}^{2L} W_i^{(c)} \left(\hat{\mathbf{x}}^{(\mathbf{i})}_{\mathbf{n+1|n}} - \hat{\mathbf{x}}_{\mathbf{n}}\right) \left(\hat{\mathbf{x}}^{(\mathbf{i})}_{\mathbf{n+1|n}} - \hat{\mathbf{x}}^{\natural}_{\mathbf{n+1|n}}\right)^T \tag{74}$$

6. The smoother gain is given by :

$$\mathbf{K}^{\natural}_{\mathbf{n}} = \hat{\mathbf{S}}^{\natural}_{\mathbf{n+1|n}} \left(\hat{\mathbf{P}}^{\natural}_{\mathbf{n+1|n}}\right)^{-1} \tag{75}$$

7. The smoothed mean is computed as :

$$\hat{\mathbf{x}}^{\natural}_{\mathbf{n}} = \hat{\mathbf{x}}_{\mathbf{n}} + \mathbf{K}^{\natural}_{\mathbf{n}} \left(\hat{\mathbf{x}}^{\natural}_{\mathbf{n+1}} - \hat{\mathbf{x}}^{\natural}_{\mathbf{n+1|n}}\right) \tag{76}$$

8. The smoothed covariance matrix is calculated by :

$$\hat{\mathbf{P}}^{\natural}_{\mathbf{n}} = \hat{\mathbf{P}}_{\mathbf{n}} + \mathbf{K}^{\natural}_{\mathbf{n}} \left(\hat{\mathbf{P}}^{\natural}_{\mathbf{n+1}} - \hat{\mathbf{P}}^{\natural}_{\mathbf{n+1|n}}\right) \left(\mathbf{K}^{\natural}_{\mathbf{n}}\right)^T \tag{77}$$

7.4. Unscented EM-algorithm

The derivation of matrices $\{\mathbf{B}_i\}, i = 1..6$ follows the same reasoning as for the Extended Kalman Filter (see [30] for details), apart from the UT that handles the nonlinear functions $f(.)$ and $g()$.

Creation of a sigma points set $\{\mathbf{x}^{(i)}_{n-1}\}$ from $\hat{\mathbf{x}}_{n-1}$ and $\hat{\mathbf{P}}_{n-1}$ by formula 60

$$\mathbf{B}_1 = \sum_{n=1}^{N} \left(\hat{\mathbf{x}}_n \hat{\mathbf{x}}_n^T + \hat{\mathbf{P}}_n\right) \tag{78}$$

$$\mathbf{B}_2 = \sum_{n=1}^{N} \sum_{i=0}^{2L} W_i^{(c)} \hat{\mathbf{x}}_n^{(i)} f\left(\hat{\mathbf{x}}_n^{(i)}\right)^T \tag{79}$$

$$\mathbf{B}_3 = \sum_{n=1}^{N} \sum_{i=0}^{2L} W_i^{(c)} f\left(\hat{\mathbf{x}}_{n-1}^{(i)}\right) f\left(\hat{\mathbf{x}}_{n-1}^{(i)}\right)^T \tag{80}$$

$$\mathbf{B}_4 = \sum_{n=1}^{N} \mathbf{y}_n \mathbf{y}_n^T \tag{81}$$

$$\mathbf{B}_5 = \sum_{n=1}^{N} \sum_{i=0}^{2L} W_i^{(c)} \mathbf{y}_n g\left(\hat{\mathbf{x}}_n^{(i)}\right) \tag{82}$$

$$\mathbf{B}_6 = \sum_{n=1}^{N} \sum_{i=0}^{2L} W_i^{(c)} g\left(\hat{\mathbf{x}}_n^{(i)}\right) g\left(\hat{\mathbf{x}}_n^{(i)}\right)^T \tag{83}$$

8. References

[1] A. Preumont, Vibration Control of Active Structures, An Introduction, Springer, 2011.

[2] K. Worden, R. Tomlinson, Nonlinearity in Structural Dynamics Detection, Identification and Modelling, Institute of Physics Publishing, 2001.

[3] G. Kerschen, K. Worden, A. F. Valakis, J.-C. Golinval, Past, present and future of nonlinear system identification in structural dynamics, Mechanical Systems and Signal Processing 20 (2006) 505–592.

[4] L. Ljung, System identification Theory for the User, Thomas Kailath, 1999.

[5] T. Söderström, P. Stoica, System identification, 2001.

[6] D. J. Ewins, Modal Testing : Theory and Practice, Research Studies Pr, 1984.

[7] A. Vakakis, O. V. Gendelman, L. A. Bergman, D. M. McFarland, G. Kerschen, Y. S. Lee, Nonlinear Targeted Energy Transfer in Mechanical and Structural Systems, Springer, 2009.

[8] G. Kerschen, M. Peeters, J. G. Golinval, V. Vakakis, Nonlinear normal modes, part I: A useful framework for the structural dynamicist, Mechanical Systems and Signal Processing 23 (2009) 170–194.

[9] P. Maragos, J. Kaiser, T. Quatieri, On separating amplitude from frequency modulations using energy operators, Acoustics, Speech, and Signal Processing, IEEE International Conference on 2 (1992) 1–4.

[10] P. Maragos, J. Kaiser, T. Quatieri, Energy separation in signal modulations with application to speech analysis, Trans. Sig. Proc. 41 (10) (1993) 3024–3051.

[11] M. Feldman, Non-linear free vibration identification via the Hilbert transform, Journal of Sound and Vibration 208 (3) (1997) 475–489.

[12] M. Feldman, Hilbert transform in vibration analysis, Mechanical Systems and Signal Processing 25 (2011) 735–802.

[13] E. Bedrosian, A product theorem for Hilbert transforms, Tech. rep., Memorandum RM-3439-PR, U.S. Air Force Project RAND (1962).

[14] A. Nuttall, E. Bedrosian, On the quadrature approximation to the Hilbert transform of modulated signals, Proceedings of the IEEE 54 (10) (1966) 1458 – 1459.

[15] J. Brown, J.L., A Hilbert transform product theorem, Proceedings of the IEEE 74 (3) (1986) 520 – 521.

[16] N. E. Huang, Z. Shen, S. R. Long, M. C. Wu, H. H. Shih, Q. Zheng, N.-C. Yen, C. C. Tung, H. H. Liu, The Empirical Mode Decomposition and the Hilbert spectrum for nonlinear and non-stationary time series analysis, Proceedings of the Royal Society of London. Series A: Mathematical, Physical and Engineering Sciences 454 (1971) (1998) 903–995.

[17] N. E. Huang, Z. Shen, S. R. Long, A new view of nonlinear water waves: the Hilbert spectrum, Annual Review of Fluid Mechanics 31 (1) (1999) 417–457.

[18] N. E. Huang, Z. Wu, A review on Hilbert-Huang transform: method and its applications to geophysical studies, Reviews of Geophysics 46 (2) (2008) n/a–n/a.

[19] J. Lardies, S. Gouttebroze, Identification of modal parameters using the wavelet transform, International Journal of Mechanical Sciences 44 (2002) 2263–2283.

[20] P. Argoul, T.-P. Le, Instantaneous indicator of structural behaviour based on the continuous Cauchy wavelet analysis, Mechanical Systems and Signal Processing 17 (1) (2003) 243–250.

[21] L. Heller, E. Foltete, J. Piranda, Experimental identification of non-linear dynamic properties of built-up structures, Journal of Sound and Vibration 327 (2009) 183–196.

[22] M. Peeters, G. Kerschen, J.-C. Golinval, Modal testing of nonlinear vibrating structures based on nonlinear normal modes : experimental demonstration, Mechanical Systems and Signal Processing 25 (2011) 1227–1247.

[23] J.-L. Dion, C. Stephan, G. Chevallier, H. Festjens, Tracking and removing modulated sinusoidal components; a solution based on the kurtosis and the extended Kalman filter, Mechanical Systems and Signal Processing 38 (2013) 428–439.

[24] R. E. Kalman, A new approach to linear filtering and prediction problems, Transactions of the ASME - Journal of Basic Engineering 82 (Series D) (1960) 35–45.

[25] M. S. Grewal, A. P. Andrews, Kalman Filtering Theory and Practice Using MATLAB, John Wiley & Sons, 2008.

[26] S. J. Julier, The scaled unscented transformation, in: Proceedings of the American Control Conference, 2002, pp. 4555–4559.

[27] S. J.Julier, J. K.Uhlmann, Unscented filtering and nonlinear estimation, Proceedings of the IEEE 92 (3) (2004) 401–422.

[28] S. Sarrka, Unscented Rauch-Tung-Striebel smoother, IEEE Transactions on Automatic Control 53 (3) (2008) 845–849.

[29] R. H. Shumway, D. S. Stoffer, Time Series Analysis and Its Applications, Springer, 2005.

[30] V. A. Bavdekar, A. P. Deshpande, S. C. Parwardhan, Identification of process and measurement noise covariance for state and parameter estimation using extended Kalman filter, Journal of Process Control 21 (2011) 585–601.

[31] P. R. Dahl, Solid friction damping of mechanical vibrations, AIAA Journal 14 (12) (1976) 1675–1682.

[32] D. Wagg, S. Neild, Nonlinear vibration with control for flexible and adaptive structures, 2009.

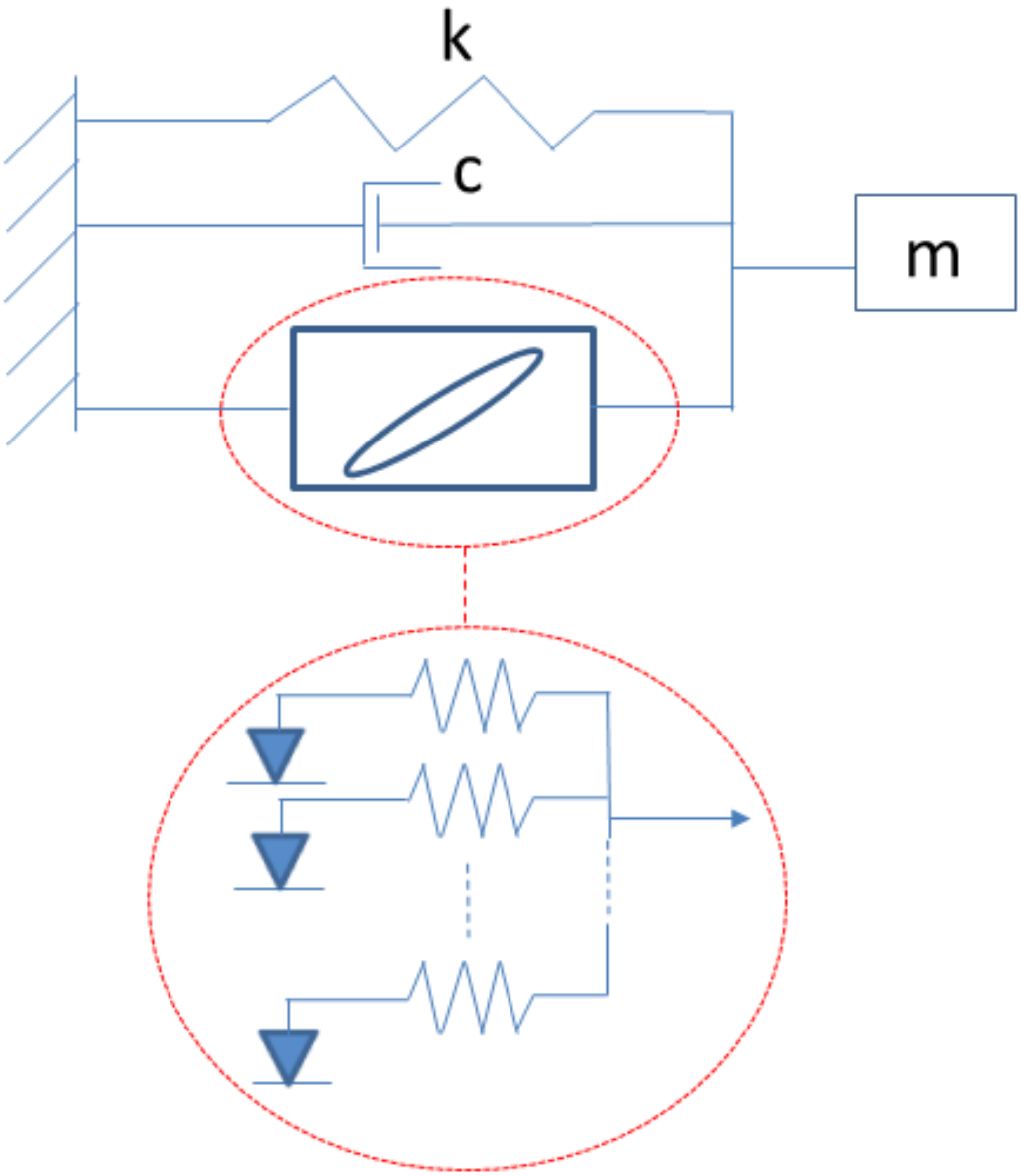

Figure 1: Iwan model

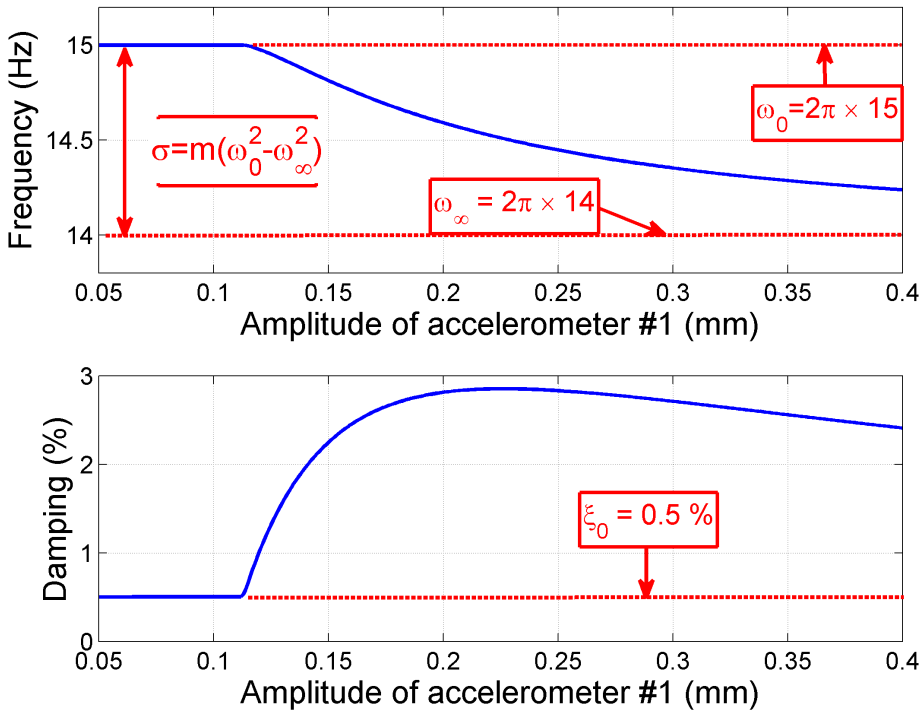

Figure 2: Equivalent modal parameters for the model example

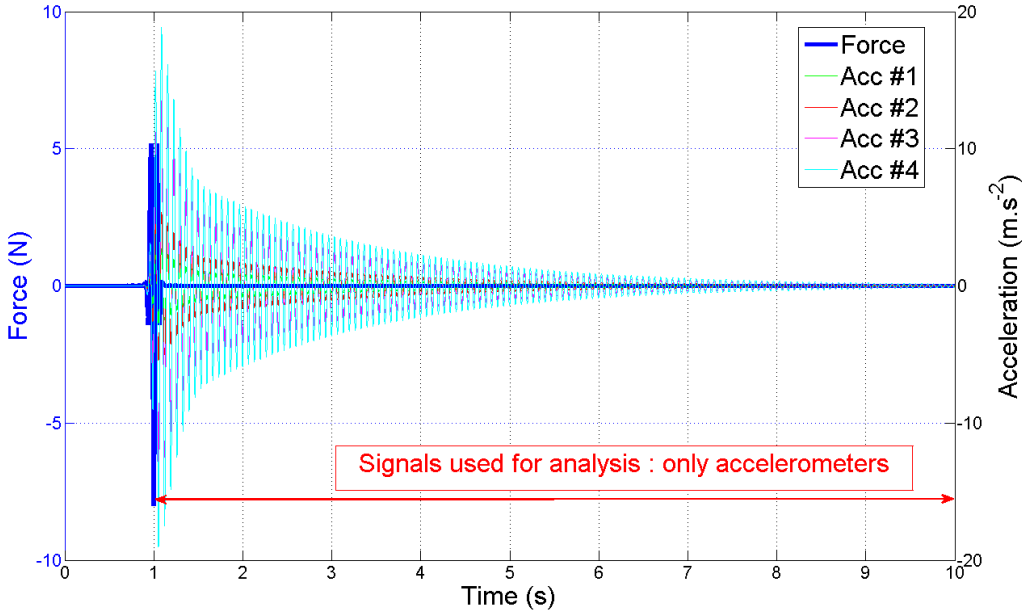

Figure 3: Response due to a wavelet excitation

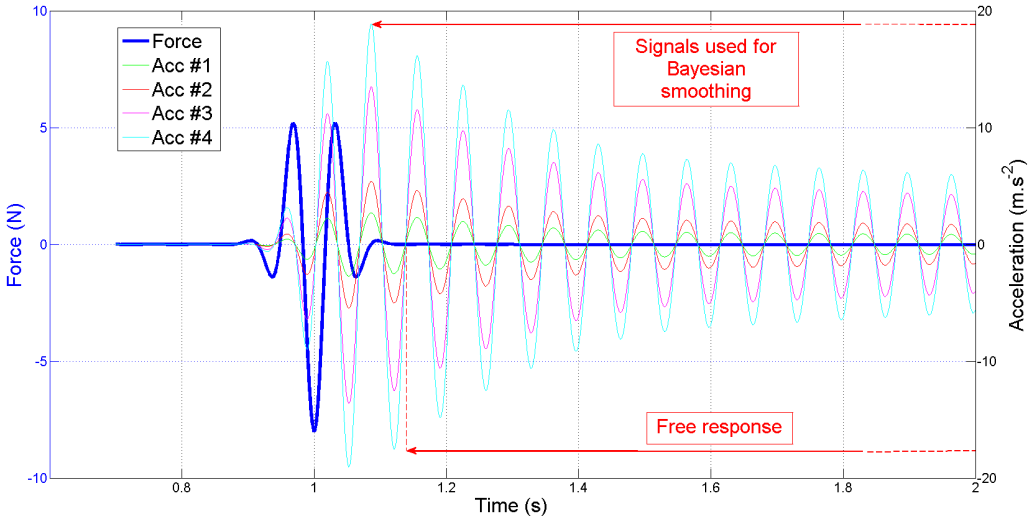

Figure 4: Zoom on the transient part due to excitation

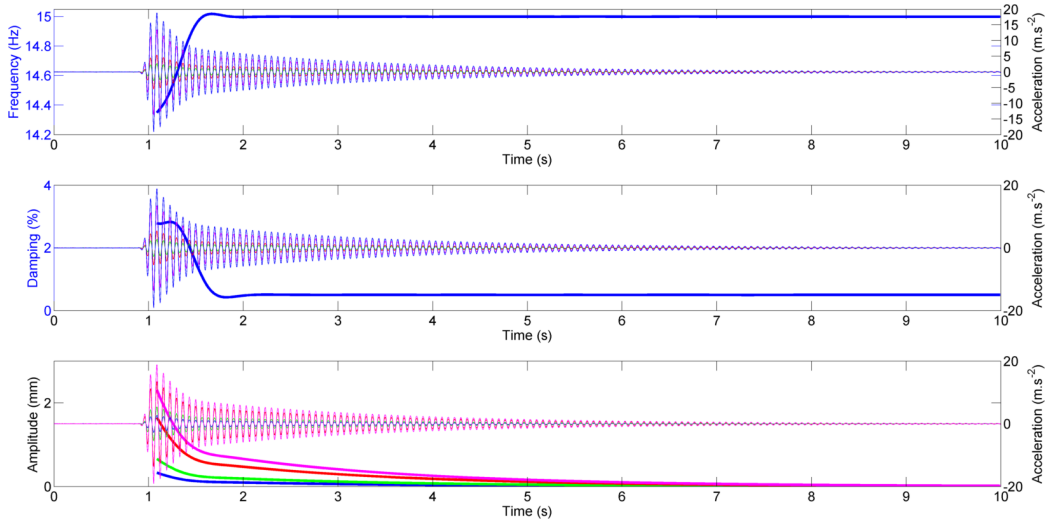

Figure 5: Equivalent modal parameters and amplitudes as a function of time

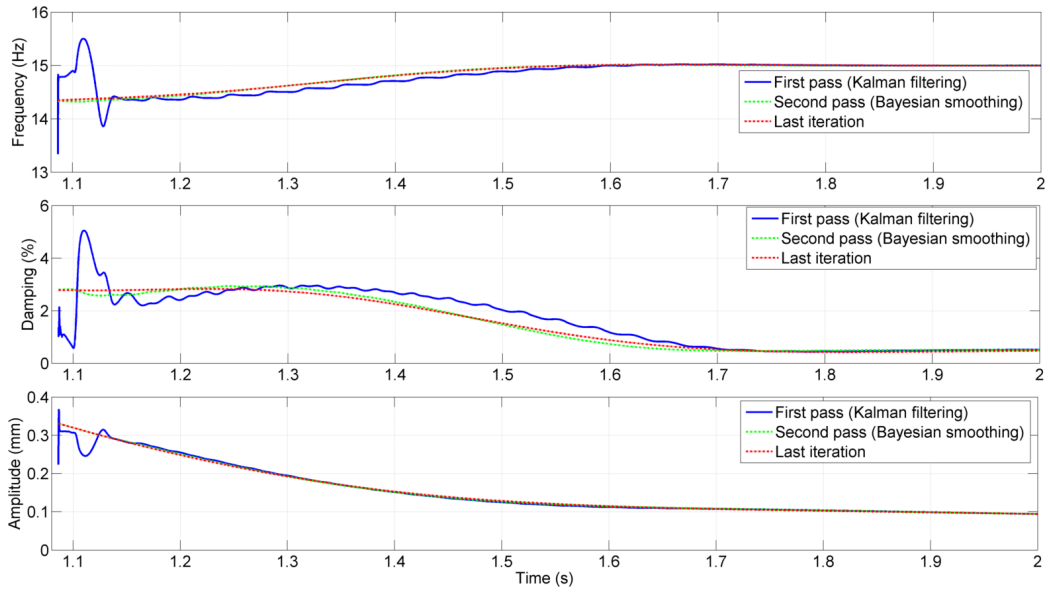

Figure 6: Equivalent modal parameters and amplitudes as a function of time : frequency, damping and amplitude of accelerometer 1

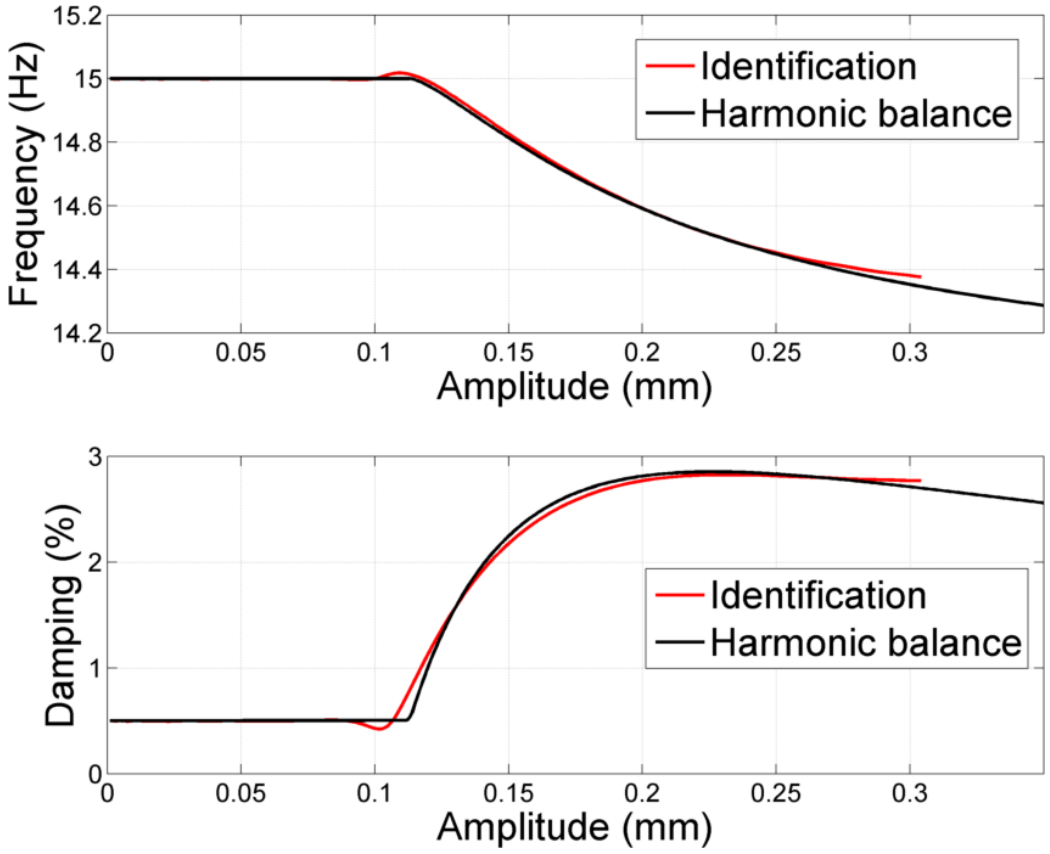

Figure 7: Equivalent modal parameters as a function of accelerometer 1 amplitude

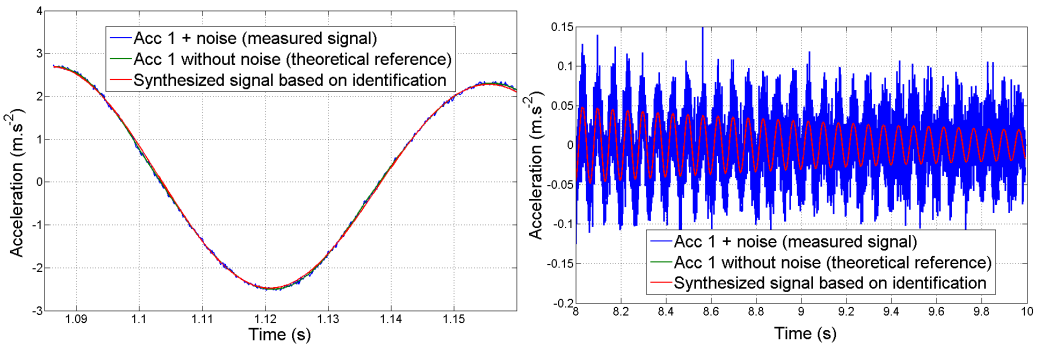

Figure 8: Measured, theoretical and synthesized acceleration signals : accurate matching of theoretical and synthesized accelerations, at beginning and end

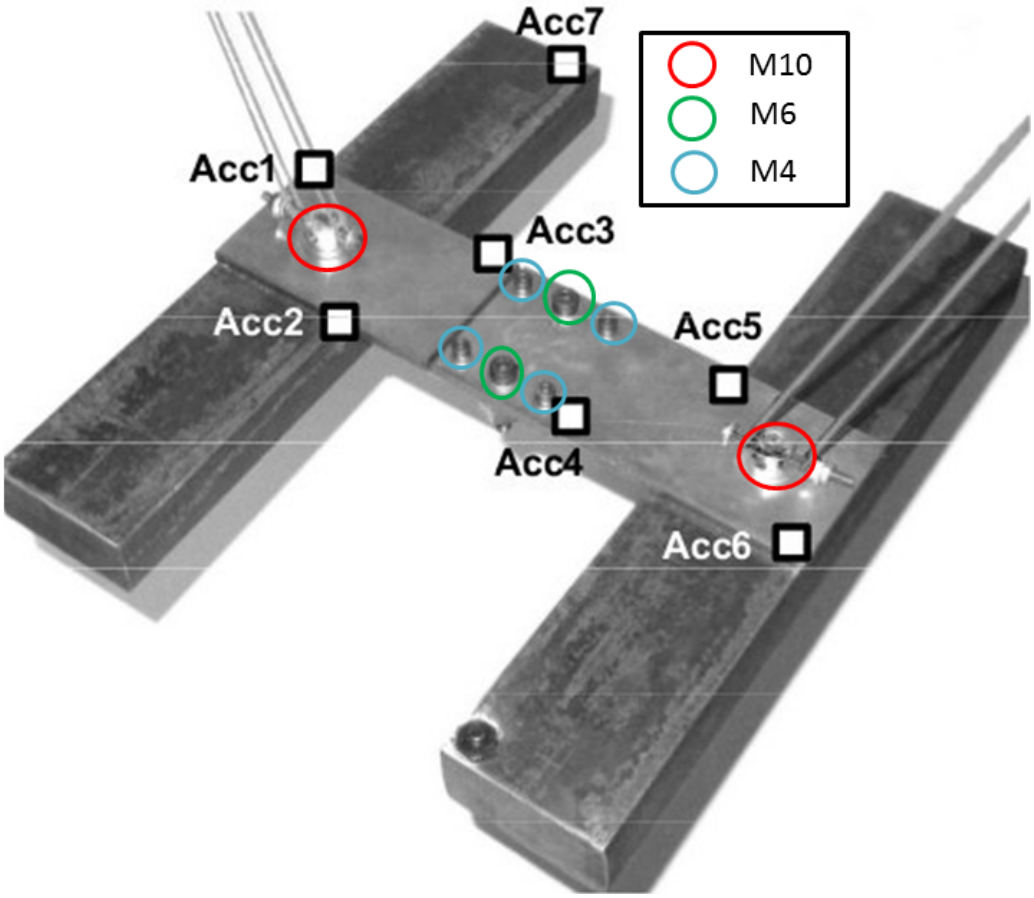

Figure 9: H Testbench

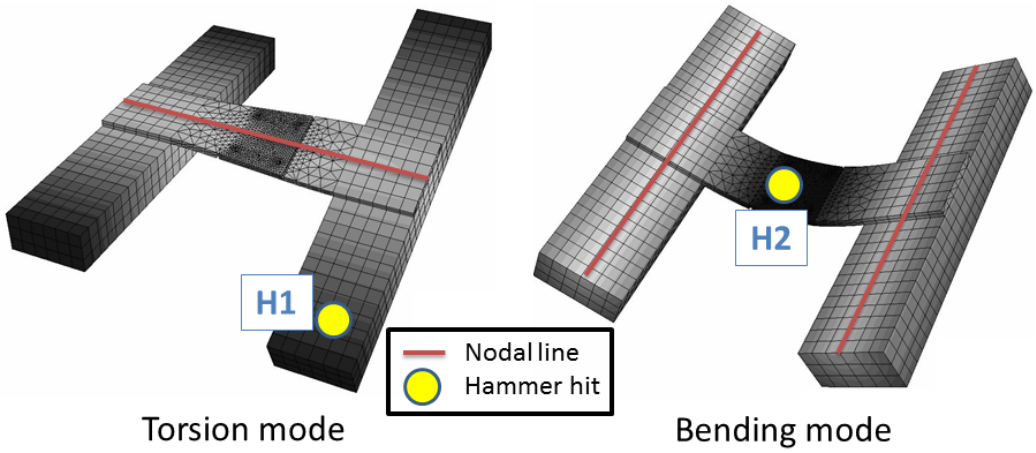

Figure 10: Torsion and bending modes

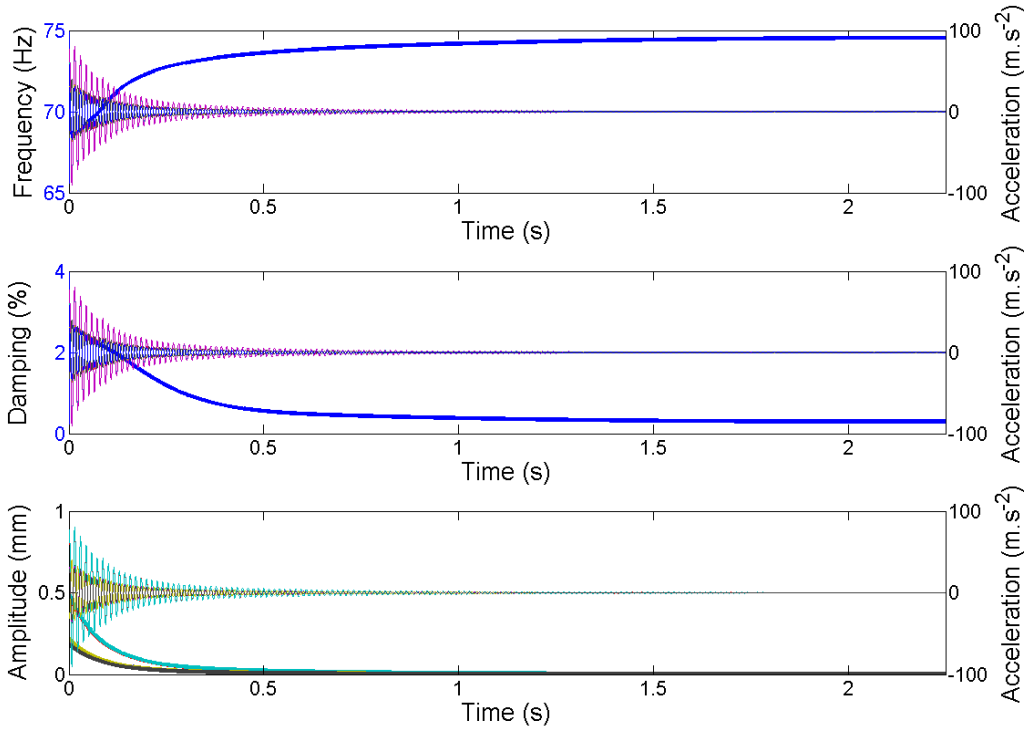

Figure 11: Equivalent modal parameters and amplitudes of the bending mode as a function of time (torque of 2 Nm)

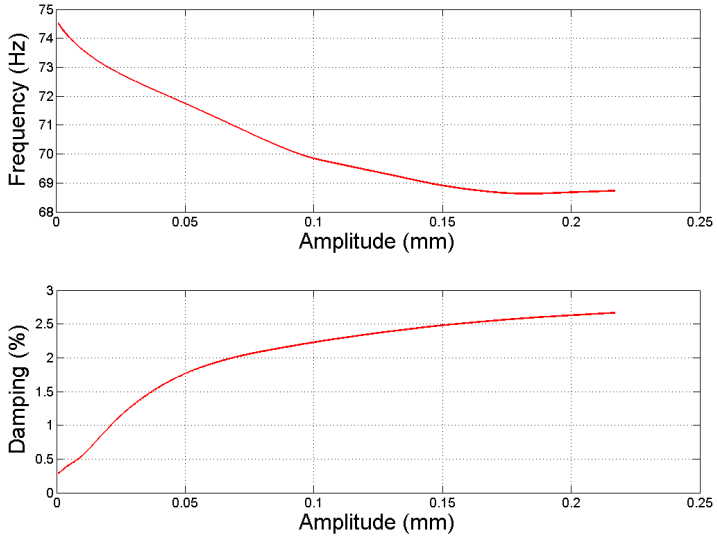

Figure 12: Equivalent modal parameters of the bending mode as a function of Acc1 displacement (torque of 2Nm)

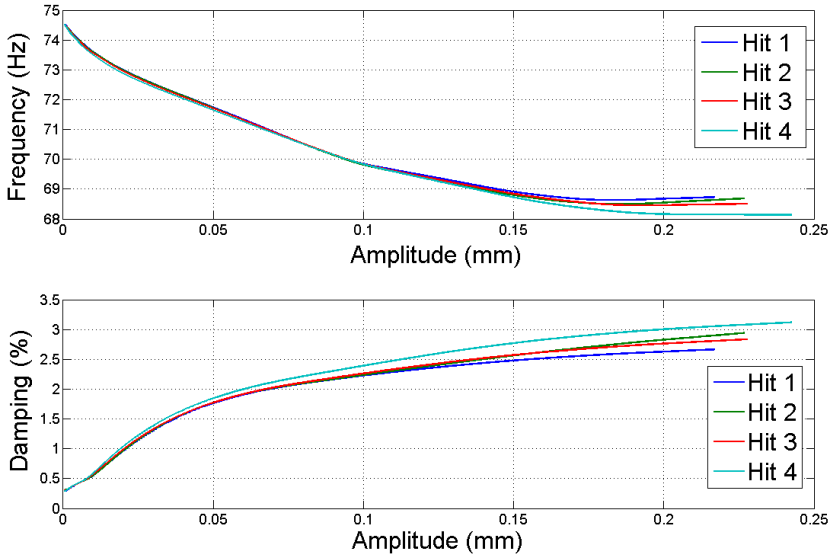

Figure 13: Repeatability of tests

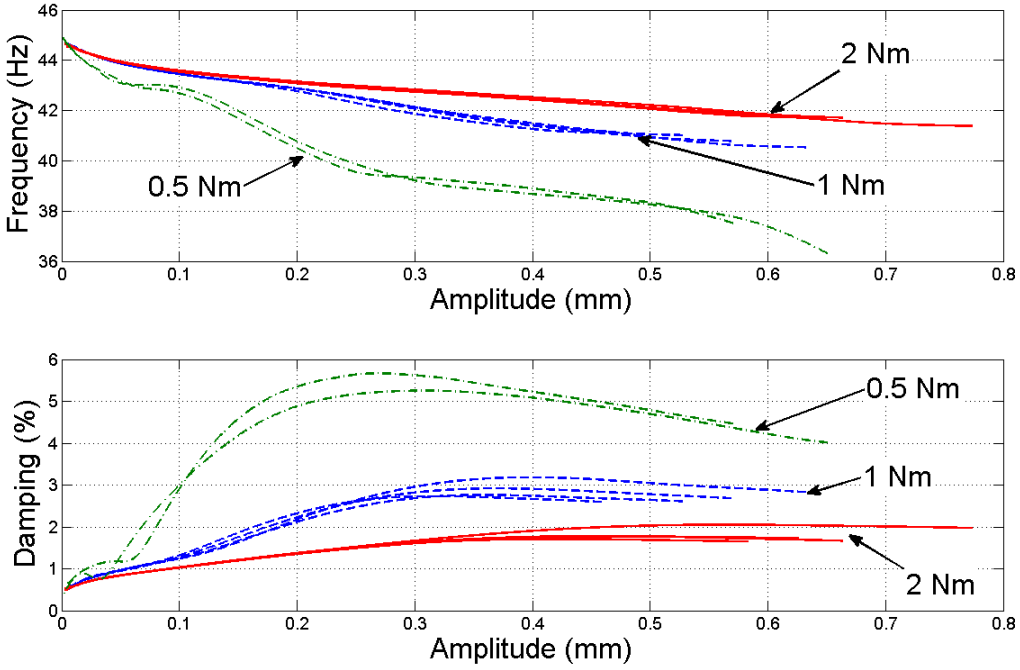

Figure 14: Equivalent modal parameters of the torsion mode as a function of Acc7 displacement